JACS Au
AN OPEN ACCESS JOURNAL OF THE AMERICAN CHEMICAL SOCIETY

pubs.acs.org/jacsau

Article

Structure Activity Relationships for Reversible O_2 Chemisorption by the Solid Phases of Co(salen) and Co(3F-salen)

Mads Sondrup Møller and Christine J. McKenzie*

Cite This: *JACS Au* 2023, 3, 1484−1495

Read Online

ACCESS | Metrics & More | Article Recommendations | Supporting Information

ABSTRACT: The potential of solid-state materials comprising Co(salen) units for concentrating dioxygen from air was recognized over 80 years ago. While the chemisorptive mechanism at the molecular level is largely understood, the bulk crystalline phase plays important, yet unidentified roles. We have reverse crystal-engineered these materials and can for the first time describe the nanostructuring requisite for achieving reversible O_2 chemisorption by Co(3R-salen) R = H or F, the simplest and most effective of the many known derivatives of Co(salen). Of the six phases of Co(salen) identified, α-ζ: α = ESACIO, β = VEXLIU, γ, δ, ε, and ζ (this work), only γ, δ, ε, and ζ are capable of reversible O_2 binding. Class I materials (phases γ, δ, and ε) are obtained by desorption (40−80 °C, atmospheric pressure) of the co-crystallized solvent from Co(salen)·(solv), solv = $CHCl_3$, CH_2Cl_2, or 1.5 C_6H_6. The oxy forms comprise between 1:5 and 1:3 O_2:[Co] stoichiometries. Class II materials achieve an apparent maximum of 1:2 O_2:Co(salen) stoichiometries. The precursors for the Class II materials comprise [Co(3R-salen)(L)·$(H_2O)_x$], R = H, L = pyridine, and x = 0; R = F, L = H_2O, and x = 0; R = F, L = pyridine, and x = 0; R = F, L = piperidine, and x = 1. Activation of these depends on the desorption of the apical ligand (L) that templates channels through the crystalline compounds with the Co(3R-salen) molecules interlocked in a Flemish bond brick pattern. The 3F-salen system produces F-lined channels proposed to facilitate O_2 transport through the materials through repulsive interactions with the guest O_2. We postulate that a moisture dependence of the activity of the Co(3F-salen) series is due to a highly specific binding pocket for locking in water via bifurcated hydrogen bonding to the two coordinated phenolato O atoms and the two *ortho* F atoms.

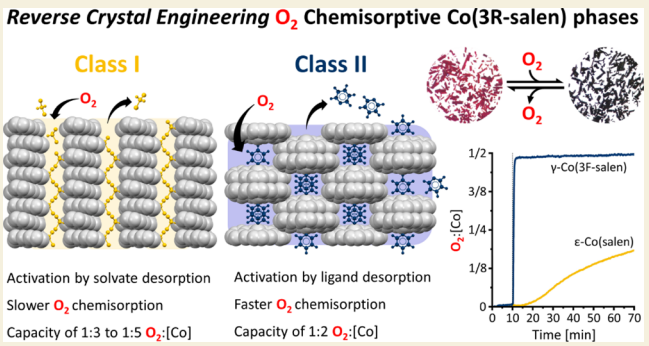

KEYWORDS: *Co(salen), dioxygen, chemisorption, gas−solid reaction, crystal engineering*

INTRODUCTION

In 1933, Pfeiffer *et al.* were the first to report the quintessential ligand *N*,*N*′-bis(salicylidene)ethylenediamine (H_2salen) and that solutions of its cobalt(II) complex changed color from red to brown/black on standing in air.[1] That this was due to a slow reaction with O_2 was deduced 5 years later by Tsumaki who demonstrated that the reaction also occurs in the solid state. When oxygenated Co(salen) was heated in a stream of carbon dioxide, the brown/black compound would return to a red color.[2] Co(salen) was, therefore, the first example of a synthetic reversible O_2-binding complex and a landmark model for the reversible oxygenation mechanism of hemoglobins. The realization that this potentially highly useful function was accessible for a synthetic compound and importantly in the solid state paved the way for proposing practical energy-saving swing absorption technologies for separating molecular oxygen from air. This goal motivated the U.S. National Defense Research Committee[3] sponsored work by Calvin who described the reactivity of 57 cobalt(II) complexes in the solid state toward O_2, including 42 salen-derived complexes, in two patents,[4,5] a book,[6] and a series of articles published after World War II.[7−15] Intriguingly, out of this extensive study, occasionally on the kilogram scale, only Co(salen) and Co(3F-salen) (3F-salen = *N*,*N*′-ethylene-bis(3-flourosalicylideneiminato)) were ultimately patented by Calvin,[4,5,16] suggesting that these complexes were deemed the most active. Since this seminal work, the Co(salen) scaffold has been studied extensively in numerous modifications incorporating, *e.g.*, electron withdrawing and donating groups and bulky substituents, in a continuing search for practical materials containing this unit.[17−26] A prevailing observation was that a ligand *trans* to the O_2 binding site tunes this function, reminiscent of the O_2 binding heme enzymes. Indeed, when dissolved in non-coordinating solvents, Co^{II}(salen) does not bind O_2 strongly without the additional stabilization of the

Received: March 21, 2023
Revised: April 19, 2023
Accepted: April 20, 2023
Published: May 4, 2023

https://doi.org/10.1021/jacsau.3c00134
JACS Au 2023, 3, 1484−1495

Scheme 1. Map of Transformations between Precursor Compounds and the Deoxy and Oxy Forms of Co(salen) and Co(3F-salen)[a]

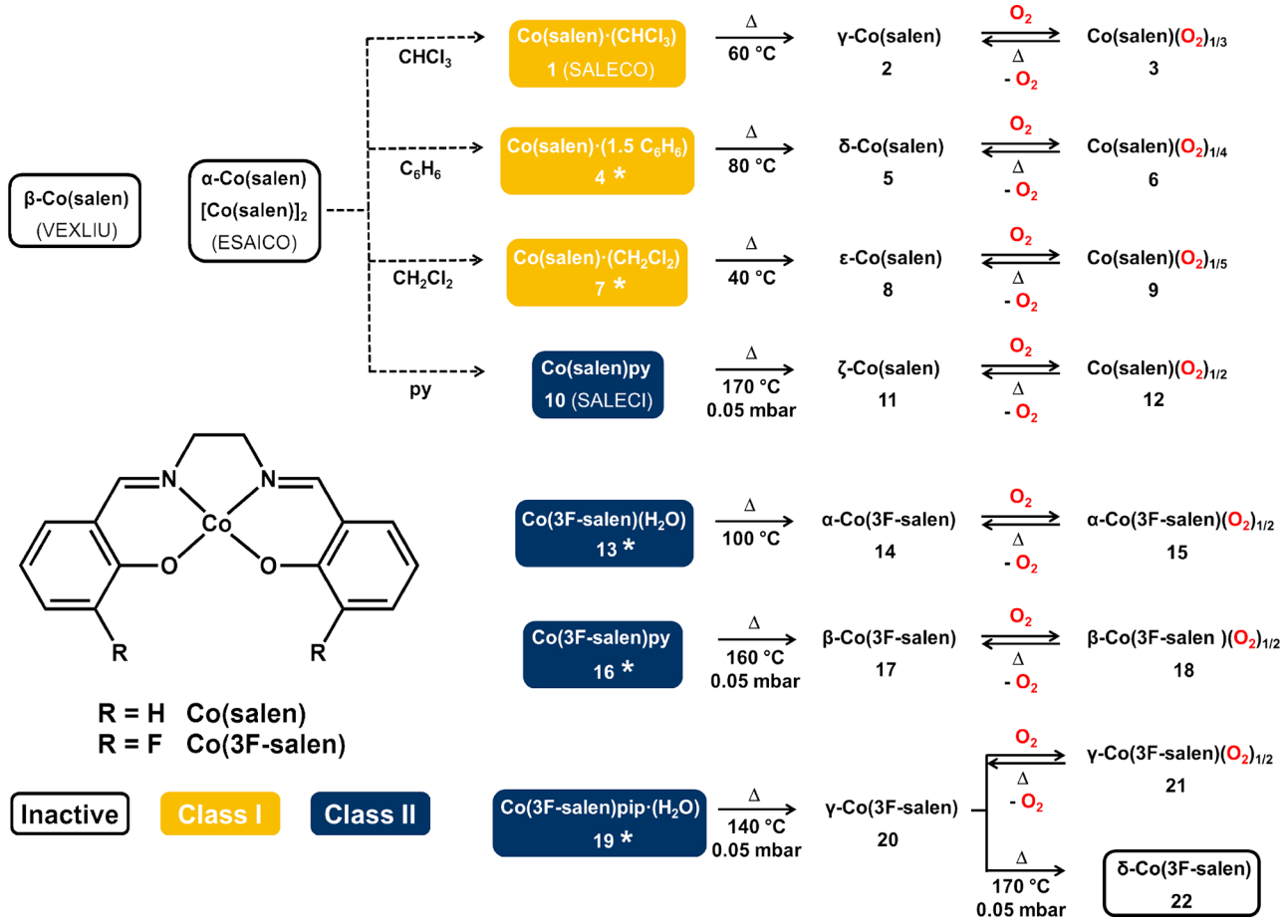

[a]Dashed and solid arrows represent solution- and solid-state reactions, respectively. py = pyridine, pip = piperidine. Phases with new single-crystal structures are denoted by an asterisk, and known structures are denoted by their CCDC ref codes. The orange and blue boxes for a particular phase indicate that it contains the specific Class I or II nanostructuring that we have identified as important for selective and reversible O_2 binding.

$Co^{III}-O_2$ bond by the increase in electron density at the cobalt center induced by a *trans* coordinating ligand.[27,28]

The measurement of O_2 affinity has however been mainly confined to the solution state, and attesting to the ease and repeatability of these observations, an experiment for undergraduate laboratory courses using Co(salen) dissolved in donor solvents (DMSO or DMF) to reversibly bind O_2 was published in 1977.[29]

In 1969, the first crystal structures of oxygenated Co(salen) complexes were reported by Randaccio *et al.*[30] and Wang and Schaefer.[31] On the basis of the structural parameters, in particular the O−O bond length, $\{[Co(salen)dmf_2]_2O_2\}$ and $\{[(H_2O)Co(3F\text{-}salen)-O_2-Co(3F\text{-}salen)]_2\cdot(CHCl_3)_2\cdot(C_5NH_{11})\}$ (the latter notably obtained by recrystallizing a sample originally synthesized by Calvin's group in 1943) were assigned as a peroxide and a superoxide complex, respectively. Although not quantified or cycled, it was concluded that these compounds lose O_2 from the bulk solid state on heating and resorb O_2 from air on cooling according to the color changes observed for both these materials. It is important to note however that there was no mention of bulk homogeneity or confirmation that the single-crystal structure was indeed representative of the bulk materials. The structures of several Co(salen)-type peroxides and superoxides, typically displaying bridging (μ:η,$^1\eta^2$-O_2^{2-})[32] and end-on (η^1-O_2^-)[33−42] structures, respectively, with bulk structural integrity often supported by vibrational spectroscopy, have been reported since.

Solid materials that reversibly bind O_2 remain of no less interest today. Materials that chemisorb O_2 will offer advantages compared to those currently used in the established pressure swing adsorption processes for concentrating O_2 from other gases using zeolites. Zeolites have voids and large internal surface areas, relying on the kinetic radii of gaseous guests and van der Waals interactions to achieve separation, which often requires several sequential cycles.[43] Chemisorption is a different mechanism that increases selectivity and affinity via direct covalent bonding. This can be confined to the surface of material (adsorptive) or a bulk (absorptive) process, which will achieve higher loadings. Molecular cobalt systems that can oxidatively add O_2 reversibly are promising in this regard,[44,45] and of the known systems, the unsubstituted Co(salen) can potentially store the highest amount of O_2 by weight. Here, we describe the crystal phase nanostructuring and structure−activity relationships (SARs) of previously reported materials and new phases of Co(salen) and Co(3F-salen), which facilitate reversible O_2 chemisorption in these landmark molecular materials.

https://doi.org/10.1021/jacsau.3c00134
JACS Au 2023, 3, 1484−1495

Table 1. Solvent System (or Additive) for Obtaining Specific Phases, Void Space in the Solvent-Accessible Channels, Intermolecular Co···Co Distances Obtained from SCXRD Data for the "As-Prepared" Phases, and Ratio of Chemisorbed O_2 per Co_2 Site

class	compound	solvent(additive)[a]	void space [Å^3][b]	void volume [%][c]	Co···Co distance [Å][d]	O_2:[Co]	reference
inactive	α-Co(salen)	H_2O/EtOH	0.0	0.0		0	ESAICO[46,49]
inactive	β-Co(salen)	MeOH/EtOAc	0.0	0.0		0	VEXLIU[47]
I	Co(salen)·($CHCl_3$) (**1**)	$CHCl_3$	529.8	28.7	3.45/5.21	1/3	SALECO[48]
I	Co(salen)·(1.5 C_6H_6) (**4**)	C_6H_6	809.6	39.1	3.35	1/4	this work
I	Co(salen)·(CH_2Cl_2) (**7**)	CH_2Cl_2	194.6	22.8	3.40	1/5	this work
II	Co(salen)py (**10**)	H_2O/EtOH (py)	466.9	25.7	8.71	1/2	SALECI[50]
II	Co(3F-salen)(H_2O) (**13**)	H_2O/EtOH	0.0	0.0	3.55/4.84	1/2	this work
II	Co(3F-salen)py (**16**)	H_2O/EtOH (py)	461.6	25.4	8.71	1/2	this work
II	Co(3F-salen)pip·(H_2O) (**19**)	H_2O/EtOH (pip)	525.8	26.6	11.74	1/2	this work

[a]py = pyridine and pip = piperidine. [b]Void space calculated using a 1.2 Å probe on a 0.7 Å grid[51] after in silico removal of co-crystallized organic solvent molecules (**1**, **4**, and **7**), py (**10** and **16**), pip and H_2O (**19**), and H_2O (**13**). [c]Percentage of unit cell volume. [d]Intermolecular Co···Co distance between cobalt atoms where an O_2 molecule is most likely to insert.

RESULTS AND DISCUSSION

Scheme 1 shows a map of the interrelationships of O_2-active and inactive phases of Co(3R-salen) R = H or F compounds that we have delineated in a revisitation of the work described predominantly by Tsumaki and Calvin in the 1930s and 1940s. By interpreting descriptive observations and repeating the syntheses originally described, in combination with single-crystal and powder X-ray diffraction (SCXRD and PXRD), IR spectroscopy, and thermogravimetric and gravimetric analyses (TGA and GA), we have deduced and identified several phases of these materials, which are named as depicted in the scheme. We have categorized these phases into two classes, I and II, based on chemical properties and structural features. This work demonstrates that the crystal phase impacts significantly on the reversible O_2 chemisorptive property in ways that can override any electronic tuning that may otherwise have been beneficial in solution.

Structures of Co^{II}(salen) Precursors

The crystal structures of two phases of Co(salen) are known. One contains dimeric units, $[Co(salen)]_2$ (ESACIO; Figure S2),[46] and the other contains monomers (VEXLIU; Figure S3).[47] We name these α-Co(salen) and β-Co(salen), respectively. Neither phase contains any void space (Table 1), suggesting that the inability of either of these phases to chemisorb O_2 in the solid state is due to inaccessibility to the cobalt(II) centers. An important point to recognize however is that the inability to chemisorb O_2 is not necessarily due to the presence of the $[Co(salen)]_2$ dimer in α-Co(salen). The production of homogeneously pure samples of these phases is controlled by using ethanol/water[13,29] or ethyl acetate/methanol,[47] respectively, as the solvent in the reaction of H_2salen and cobaltous acetate under an inert atmosphere. α-Co(salen) can be stored for prolonged periods of time (years) without suffering air oxidation and proved to be a convenient starting material for the preparation of the O_2-active phases of Co(salen) we describe here.

Class I O_2 Active Phases: γ-, δ-, and ε-Co(salen)

The Co(salen) materials first recognized by Tsumaki to sorb O_2 from air were described as being obtained from the recrystallization of Co(salen) from chloroform or benzene under an inert atmosphere.[2] We have repeated this and confirm that chloroform and benzene solvates of Co(salen) are isolated, which after heat conditioning, generate O_2 active phases. The crystal structure of Co(salen)·($CHCl_3$) (**1**) is known,[48] and structures of the benzene and a new dichloromethane solvate, which similarly generates active phases, Co(salen)·(1.5C_6H_6) (**4**; Figure S4a and Table S1), and Co(salen)·(CH_2Cl_2) (**7**; Figure S4b and Table S1), are reported here. The feature common to **1**, **4**, and **7** is stacks of Co(salen) molecules surrounded by columns of well-ordered co-crystallized solvent molecules (Figure 1). The orientation of the Co(salen) molecules alternates in the stacks with each molecule rotated by 180° about the CoN_2O_2 plane with respect to its neighbors. In all three structures, the

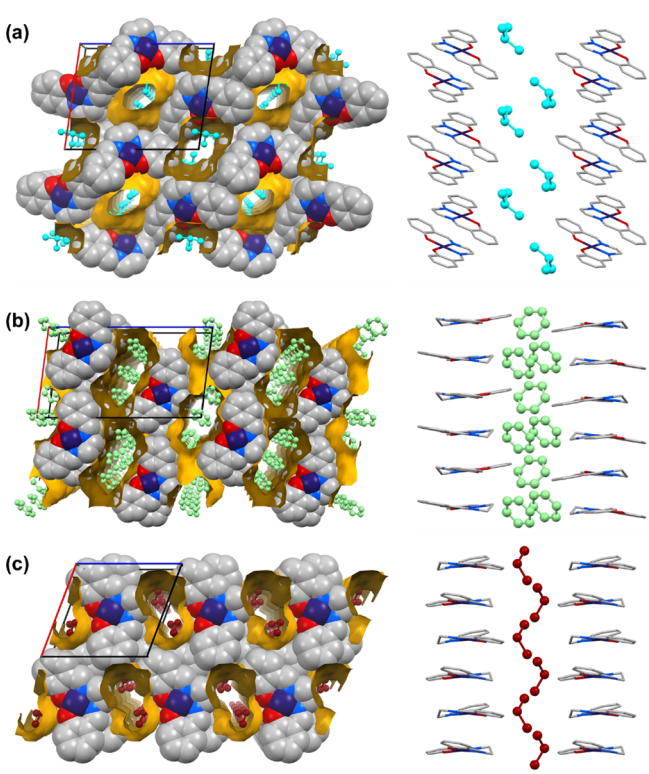

Figure 1. Crystal packing along the *b* axis (left) showing the surfaces of the solvent-accessible voids as gold-colored surfaces containing the co-crystallized solvent molecules ($CHCl_3$, cyan; C_6H_6, green; and $CHCl_2$, burgundy) superimposed and stacks of Co(salen) showing solvent channels for each phase running parallel to the *b* axis (right) for (a) Co(salen)·($CHCl_3$) (**1**) (data obtained from SALECO),[48] (b) Co(salen)·(1.5 C_6H_6) (**4**), and (c) Co(salen)·(CH_2Cl_2) (**7**).

https://doi.org/10.1021/jacsau.3c00134
JACS Au 2023, 3, 1484−1495

columns run parallel to the *b* axis. For **4** and **7**, the CoN_2O_2 plane of the Co(salen) molecules lies perpendicular to this axis while they are tilted by 74.5° in **1**. In turn, this controls the intermolecular Co···Co distances: The phases **4** and **7** show single intermolecular Co···Co distances of 3.35 and 3.40 Å, respectively, while **1** shows alternating Co···Co distances of 3.45 and 5.21 Å (Figure 1 and Table 1). The benzene molecules of **4** interact with each other through T-shaped C−H···π interactions with C−H···benzene centroid distances of 2.76 and 3.25 Å (Figure S5). The organochlorides in **1** and **7** show weak non-classical hydrogen bonding with the phenolato O atoms (O_{ph}···H−CCl_3 2.50 Å and O_{ph}···H−$CHCl_2$ 2.42 Å).

Consistent with O_2 chemisorption and concurrent cobalt(II) oxidation in an oxidative addition reaction, if left in air, then crystals of **1**, **4**, and **7** gradually change color from red (**1** and **7**) and brown (**4**) to brownish black over 30 min to 24 h, depending on the crystal size (Figure S6). The lack of strong interactions between the co-crystallized solvent and the host structure is consistent with facile desorption of the co-crystallized solvent molecules, which does not require vacuum. It seems reasonable that the channels traversing the materials in which the solvents are located are also those where O_2 enters and diffuses through the structures. In silico removal of the solvent molecules from the structures of **1**, **4**, and **7** indicates that hypothetical channels account for 23−39% of the total unit cell volume (Table 1). The crystals of the precursor phases **1**, **4**, and **7** can be heated in a stream of nitrogen (100 °C, 30 min) to yield their corresponding O_2 active phases γ-Co(salen) (**2**), δ-Co(salen) (**5**), and ε-Co(salen) (**8**), or they can be left in a stream of O_2 to give the oxygenated phases Co(salen)$(O_2)_{1/3}$ (**3**), Co(salen)-$(O_2)_{1/4}$ (**6**), and Co(salen)$(O_2)_{1/5}$ (**9**). Upon heating in a stream of nitrogen (100 °C), **3**, **6**, and **9** reform their respective active deoxy phases **2**, **5**, and **8** (Figure 2) and this is

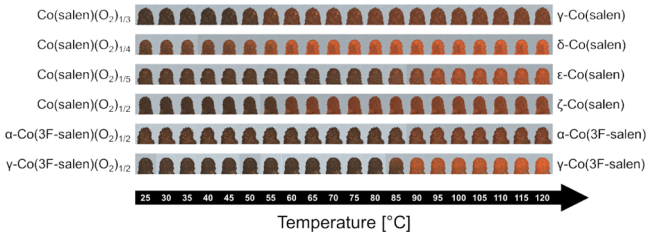

Figure 2. Color changes associated with the deoxygenation of phases of Co(3R-salen) R = H or F that occur upon heating.

accompanied by a color change from black to hues between red and brown (Figure 2). Where possible, phase changes associated with these processes were followed using variable temperature powder X-ray diffraction (VT-PXRD). The patterns show that the crystal phases change gradually upon deoxygenation, with the initial onset of the phase change occurring at 50 °C for **3** and 40 °C for **6** and **9**. Complete conversion and deoxygenation are observed at 70 °C for all three phases. Common for all the oxygenated phases are intense reflections at 2θ = 6.73°, which are retained upon deoxygenation. As the samples are heated, a second major peak grows at 2θ = 11.47°. The reflection at 2θ = 26.12° moves to 2θ = 26.45° when the sample is cooled (150−25 °C), corresponding to a slight thermal compression of the molecular planes when cooling. Upon complete deoxygenation, phases **3**, **6**, and **9** all transform to what at first glance appears to be the same crystalline phase. However, this cannot be the case since the resulting deoxygenated materials sorb O_2 at different rates and capacities (Figure 4). These materials are therefore defined as different phases and assigned the Greek prefixes: γ-, δ-, and ε-Co(salen) (Scheme 1 and Figures 2 and 3).

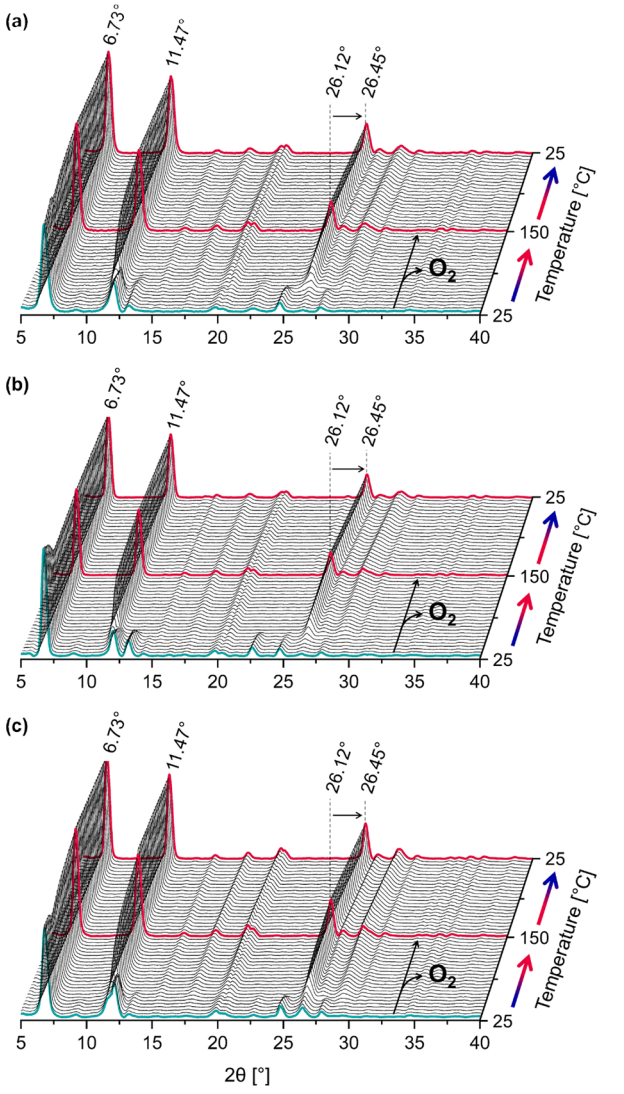

Figure 3. VT-PXRD patterns recorded while heating between 25 and 150 °C and subsequent cooling to 25 °C (blue to red and red to blue arrows, respectively) of the oxygenated phases in teal (a) Co(salen)-$(O_2)_{1/3}$ (**3**), (b) Co(salen)$(O_2)_{1/4}$ (**6**), and (c) Co(salen)$(O_2)_{1/5}$ (**9**). The corresponding active deoxy phases in red; (a) γ-Co(salen) (**2**), (b) δ-Co(salen) (**5**) and (c) ε-Co(salen) (**8**) are present at 150 °C.

γ-, δ-, and ε-Co(salen) will have dominating structural features in common, and this rationalizes why the three distinguishable precursor phases (**1**, **4**, and **7**) yield similar X-ray powder patterns for **2**, **5**, and **8** upon the desorption of solvates. Similarly, PXRD-distinguishable **3**, **6**, and **9** are obtained on oxygenation of **2**, **5**, and **8**. These features are as follows: (i) All molecules are close to planar. (ii) In **1**, **4**, and **7**, the molecules are stacked on top of each other, forming parallel columns with the layers arranged in an oblique two-dimensional parallelogram pattern and crystallize in either the $P2_1$ or $P2_1/n$ space groups. (iii) Within the stacks, the

https://doi.org/10.1021/jacsau.3c00134
JACS Au 2023, 3, 1484−1495

distances between the mean molecular planes are very similar at ∼3.35 Å corresponding to a $\pi-\pi$ stacking distance. (iv) The two most intense reflections for all the deoxygenated phases are observed at 2θ = 6.73 and 11.47°. Given that *hkl* planes are determined by molecular size and unit cell dimensions, it is interesting to note that these reflections can, in theory, be related to the lateral dimensions of a planar Co(salen) molecule (13.1 Å × 7.7 Å). (v) The size and shape of the solvent-occupied channels are determined by the guest solvent. Upon desorption of the guests, these channels are likely to collapse to a similar size. (vi) In silico removal of the solvate molecules **1**, **4**, and **7** causes a loss of intensity for reflections in the calculated PXRD patterns in the region above 2θ = 10° (Figure S7). Supporting this rationalization is an analysis of solid-state 4,11-difluoroquinacridone, which like Co(salen) is a planar molecule that stacks in crystals. Indistinguishable powder patterns are produced despite differences in the calculated lattice parameters, space groups, *Z*, *Z*′, and molecular packing for four distinct calculated structural models.[52]

Reoxygenation of *γ*-, *δ*-, and *ε*-Co(salen) in air occurs significantly more slowly (several hours) compared with the initial oxygenation of the solvates **1**, **4**, and **7**; however, in a pure O_2 atmosphere, this is reduced to 30−120 min. Additionally, the rate of oxygenation and O_2 capacity depends on the phase, the phases with faster O_2 uptake also showing the highest capacity. GA reveals the following capacity and oxygenation rate in order from highest to lowest: *γ*-Co(salen) (**2**) > *δ*-Co(salen) (**5**) > *ε*-Co(salen) (**8**). The amount of O_2 absorbed by **2** corresponds roughly to 1 equiv of O_2 per three Co atoms. The crystalline oxy form is, therefore, formulated as $Co(salen)(O_2)_{1/3}$ (**3**) and is entirely consistent with Tsumaki's proposal for the stoichiometry in 1938 using manometric measurements on what we believe to be the chloroform solvate **1**. Crystalline *γ*-Co(salen) is regenerated on O_2 desorption from **3** (Figure 3). In our hands, **1** crystallizes in two morphologies, as thin rods[48] and hexagonal blocks (the phase originally described by Tsumaki)[2] (Figure S8), with the rods crystallizing first. SCXRD reveals however identical structures for the rods and the blocks. Measurements were done on mixtures since we were unsuccessful in preparing pure bulk samples of the morphologically different crystals. Occasionally, samples of **2** were observed to take up slightly more O_2 than the 1:3 ratio so it is possible that the morphology has a macroscopic effect on the O_2 capacity. For phases **5** and **8**, oxygen uptake occurs significantly more slowly, and the amount of oxygen absorbed is also lower, corresponding to 1 equiv of O_2 per four and five Co atoms, respectively. The crystalline oxy forms are, therefore, formulated as $Co(salen)(O_2)_{1/4}$ (**6**) and $Co(salen)(O_2)_{1/5}$ (**9**). Common for the active phases **2**, **5**, and **8** is that they all display a delay in the oxygen uptake from when they are first exposed to a O_2 atmosphere (Figure 4). This lag period lasts 6−15 min before any noticeable O_2 absorption is recorded, and we speculate that some sort of surface priming process occurs during this time.

The intermolecular Co···Co distances (Table 1) in the Co(salen) stacks of **1**, **4**, and **7** are not particularly appropriate for accommodating either *syn*- or *anti*-bridging peroxide ligands where M···M distances are typically ca. 3.5 and 4.5 Å, respectively.[53−57] Perhaps consistently with the presence of two intermolecular Co···Co distances (3.45 and 5.21 Å), the 1:3 O_2:[Co] stoichiometry of **3**, along with the fastest O_2 uptake by these Class I binders, can be rationalized by a small

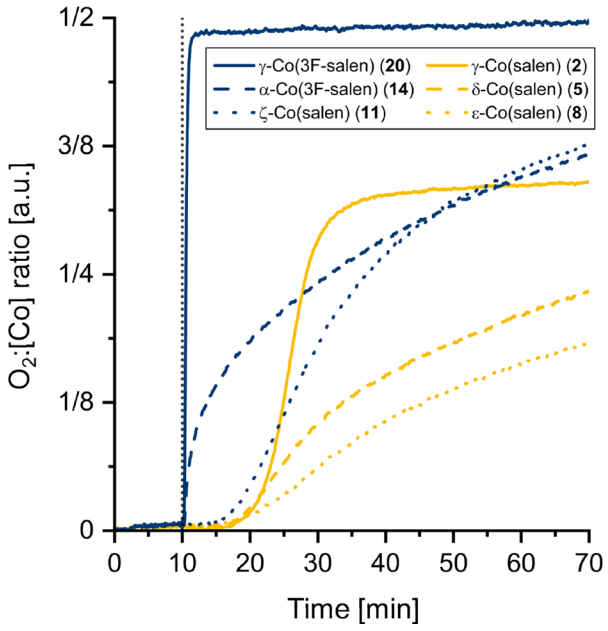

Figure 4. O_2 uptake by active phases, the black dotted line indicates the time the O_2 was turned on (25 °C, 20 mL O_2/min, 1 atm). Blue = Class II phases of Co(salen) and Co(3F-salen) and orange = Class I phases of Co(salen). GA using N_2 and then O_2 flow.

translation of the Co(salen) molecules to create the appropriate geometry for a Co−O−O−Co motif as in the depiction in Figure 5 with Co^{II}(salen) units sandwiched

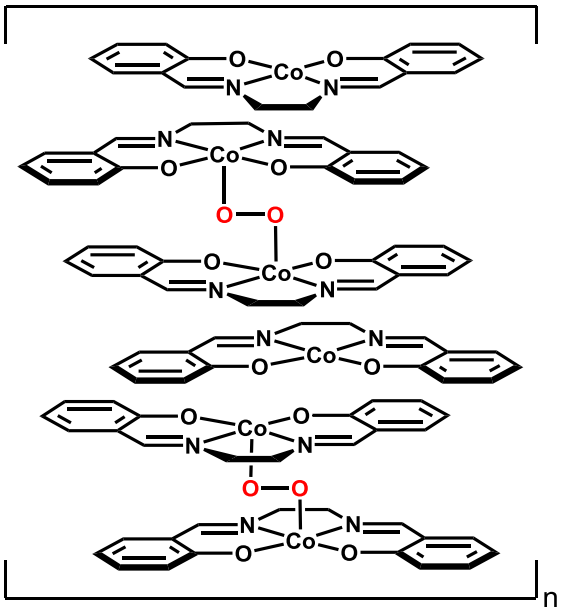

Figure 5. Illustration of the putative regular 1:3 O_2:[Co] intercalated structure for the stacks in *γ*-Co(salen) (**3**).

between (salen)Co^{III}−O−O−Co^{III}(salen) units and an *anti*-orientation for the bridging peroxide. It is notable that the *anti*-mode has been observed in a handful of structurally characterized μ_2-peroxide-di-Co(salen) complexes[32,57] that crystallize from solution. Conceivably, similarly regularly spaced O_2 insertions might generate the regular 1:4 and 1:5 O_2:[Co] stoichiometries for **6** and **9**.

https://doi.org/10.1021/jacsau.3c00134
JACS Au 2023, 3, 1484−1495

Class II O_2 Active Phases: ζ-Co(salen) and γ-, δ-, and ε-Co(3F-salen)

Co(salen)py (**10**) can be obtained from recrystallization of α-Co(salen) in pyridine (py) or prepared directly with the addition of pyridine to the reaction of cobaltous acetate and H_2salen. Unlike the Class I compounds, **10** is just as air-stable as α-Co(salen). This led Calvin to describe pyridine and piperidine (pip) as "blocking agents" due to their ability to prevent O_2 sorption.[5] The crystal structure of **10** (SALECI) showing the axially coordinated pyridine was reported in 1970.[50] Over 30 years earlier, Calvin and Bailes demonstrated that a phase that surely corresponds to **10** was activated by heating for 1.5 h at 160−220 °C under a flow of N_2.[13] Exposure of the resultant red-brown powder to oxygen or air was accompanied by a color change to jet black, and manometry measurements suggested that one molecule of O_2 per 2 moles of Co(salen) was sorbed. The pyridine desorption (170 °C, 0.05 mbar, bulk material), O_2 chemisorption (air, atmospheric pressure), and O_2 desorption (60 °C, N_2 stream) processes are completely reproducible in our hands. We have named the oxygen active phase produced by pyridine desorption from **10**, ζ-Co(salen) (**11**). The Co(salen)py units in the structure of **10** are stacked in adjacent face-to-face molecules and arranged such that the coordinated pyridines are stacked in columns with their centroids placed 3.77 Å apart. The surrounding Co(salen) molecules are packed in a Flemish bond brick pattern (Figures S9 and S10). This arrangement suggests that the desorption of pyridine will leave parallel channels traversing the structure (Figure 6a and Figure S9c) lined by exposed dicobalt (II) sites. This contrasts to the channel surfaces in **2**, **5**, and **8**, which will be more hydrophobic. The lattice structure of **10** may be important for preventing collapse of the channels created on the desorption of the pyridine. Although the orientation of the Co(salen) units is close to ideal for the incorporation of an *anti*-μ_2-peroxide ligand, the interatomic Co···Co distance is too long at 8.71 Å (Figure S7 and Table 1). Thus, either a compression must occur to form a Co^{III}−O−O−Co^{III} moiety or the space is better suited for the valence tautomer (Co^{III}−O−O$^{\cdot}$···Co^{II}). Relevant to this consideration is the ν_{O-O} at 1011 cm^{-1} that was observed in the Raman spectrum of solid oxygenated Co(salen) of the phase that we deduce from the reported preparation was **12**.[58] It is pertinent to compare this value to the ν_{O-O} stretches in the solid-state peroxide-bridged dicobalt complexes $\{[(NH_3)_5Co]_2(\mu_2\text{-}O_2)\}(SO_4)_2$,[59] {[Co(salen)DMF]$_2$($\mu_2$-$O_2$)},[58,60] oxymyoglobin,[61] and Co(*TPP*)-superoxide,[62] which appear at 808, 897, 1103, and 1287 cm^{-1}, respectively. This is therefore consistent with the bound O_2 in **12**, showing a tendency toward superoxide character. Previously, this phase has been assumed to be a peroxide.[8,13] Given the new structural information, we can speculate that the Co^{III}−O−O$^{\cdot}$···Co^{II} tautomer may be the more appropriate electronic description for the oxygenated Class II materials (Figure 6b). Additionally, the phase we believe was **12** was shown to be diamagnetic.[10] This observation does not, however, exclude either of the aforementioned electronic formulations. The magnetic susceptibility as a function of oxygenation of the phase we believe is **11** showed a linear relationship as would be expected for a two-component solid solution.[10] Relevantly, Co(salmhpn) (salmhpn = *N*,*N*′-(3,3′-dipropylmethylamine)bis(salicylideneaminato) is also active in reversible O_2 binding in the solid state.[39] In contrast to the related salen scaffold, salmhpn furnishes an inbuilt axial amine donor. Like **12**, **15**, **18**, and **21**, the oxygenated phase derived from Co(salmhpn) shows a 1:2 O_2:Co stoichiometry. This is because only one out of two molecules bear the sorbed O_2 with an O−O distance consistent with an Co^{III}-superoxide. The other molecule is the Co^{II} complex. Antiferromagnetic coupling was observed in this material.[39]

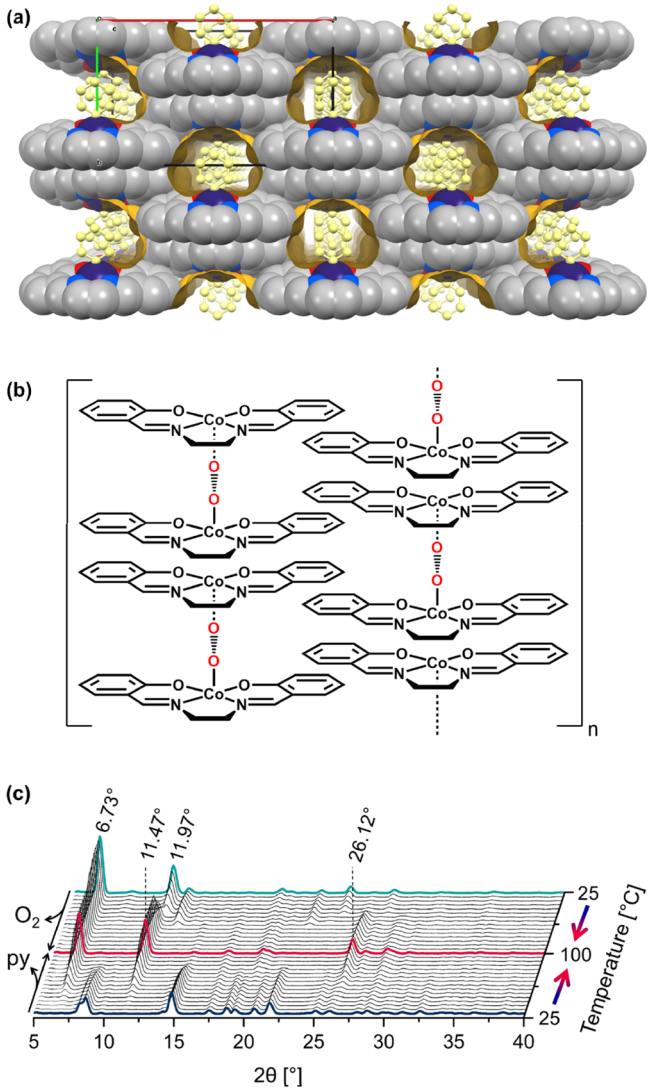

Figure 6. (a) Channels created by desorption of coordinated pyridine from Co(salen)py (**10**) using coordinates from SALECI.[50] The gold-colored surfaces represent the voids generated by in silico removal of the coordinated pyridines (yellow). (b) Illustration of the putative regular 1:2 O_2:[Co] intercalated structure for the stacks in ζ-Co(salen) (**11**). (c) VT-PXRD patterns recorded during the stepwise heating of Co(salen)py (**10**, blue) and Co(salen)$(O_2)_{1/2}$ (**12**, teal). Both processes result in the formation of ζ-Co(salen) (**11**, red).

VT-PXRD shows that the phase change associated with pyridine desorption from **10** happens gradually across a wide temperature range (45−95 °C; Figure 6c), the diffractogram of **10** fitting nicely with the calculated pattern from the crystal structure (Figure S11). The resulting oxygen active phase **11** is also a crystalline material, and its PXRD pattern shows features in common with the patterns for **2**, **5**, and **8**, consistent with column/sheet arrangements of the Co(salen) molecules. Compared to the phase change associated with desorption of pyridine, the phase change associated with deoxygenation of the crystalline Co(salen)$(O_2)_{1/2}$ (**12**) is much more sudden

https://doi.org/10.1021/jacsau.3c00134
JACS Au 2023, 3, 1484−1495

(40−50 °C). Complete deoxygenation of **12** results in reformation of **11** (Figure 6c). An initial time lag for oxygen uptake was also seen for **11**; however, this lag is a few minutes shorter compared with those for **2**, **5**, and **8**. The rate of oxygenation decreases as the material fills up, suggesting that a hopping mechanism from the Co-site to the Co-site toward the middle of the particles is likely.

Calvin and Bailes discovered that the fluorine-substituted, Co(3F-salen)-based materials showed significantly higher cycling stabilities and faster kinetics compared with all the other Co(salen) derivatives investigated. We can confirm this observation. Additionally, they reported that Co(3F-salen) forms two different hydrates, purportedly both monohydrates, although they had no proposals or evidence for structural formulation.[13] One of these, and according to Murphy's Law,[63] the one for which synthesis was irreproducible, showed a significantly faster O_2 absorption after thermal activation. There is mention of 250 attempts to repeat the synthesis.[13] Our reinvestigation of the Co(3F-salen) scaffold sheds some light on these astute observations and show that a single-water molecule can strongly associate to the Co(3F-salen) scaffold in two ways: By coordination in an apical position and through bifurcated H-bonding to the phenolate O atoms and the two fluorine atoms (Figure 7a). We have structurally characterized both these motifs separately in Co(3F-salen)(H_2O) (**13**) and Co(3F-salen)pip·(H_2O) (**19**).

The water-coordinated monohydrate is reproducibly prepared by addition of aqueous cobalt(II) acetate to a hot alcohol solution of the pro-ligand in the absence of air, to yield the red crystals of **13** (Table S2). The geometry around the cobalt atom is almost ideally square pyramidal, the angles deviating on average only 1.34° from 90° and the cobalt atom lying only 0.09 Å over the ONNO plane. It forms a dimeric structure held together by interdimer bifurcated hydrogen bonds from the axial H_2O in one unit to the phenoxy oxygen atoms and an embrace by fluorine atoms in the other molecule (O_{ph}···H−OH 2.09 Å, C−F···H−OH 2.43 Å; Figure 7b). No significant void spaces are created upon in silico removal of the water in the structure of **13** (Table 1), suggesting that the oxygenation of the activated phase occurs through nondirective diffusion of oxygen into the non-porous structure or that a rearrangement of the structure occurs upon activation resulting in channels, akin to those in **10**, running through the structure. VT-PXRD shows that the pattern of powdered **13**, which fits nicely with the pattern calculated from SCXRD data (Figure S11), changes upon heating in a stream of nitrogen. This phase change can be ascribed to the desorption of the coordinated water molecules, which occurs suddenly around 70 °C (Figure 7c). The resulting activated phase is dubbed α-Co(3F-salen) (**14**), and this phase chemisorbs 1 mol of oxygen per two cobalt centers. Heating the oxygenated phase α-Co(3F-salen)$(O_2)_{1/2}$ (**15**) in a stream of nitrogen reforms the deoxygenated phase **14**, at around 90 °C (Figure 7c). The relatively high temperature needed is due in part to the higher oxygen affinity displayed by the phases of Co(3F-salen) compared to Co(salen). In contrast to the compounds with the Co(salen) scaffolds, the oxygenation of **14** occurs almost instantaneously (Figure 4). The high rate of sorption however quickly decreases with time. Thus, **14** is on par with **11** in terms of time taken for full oxygenation to a phase with a 1:2 O_2:[Co] stoichiometry (Figure S12).

Structural analyses of the pyridine and piperidine adducts of the Co(3F-salen) scaffold are important for elucidating the

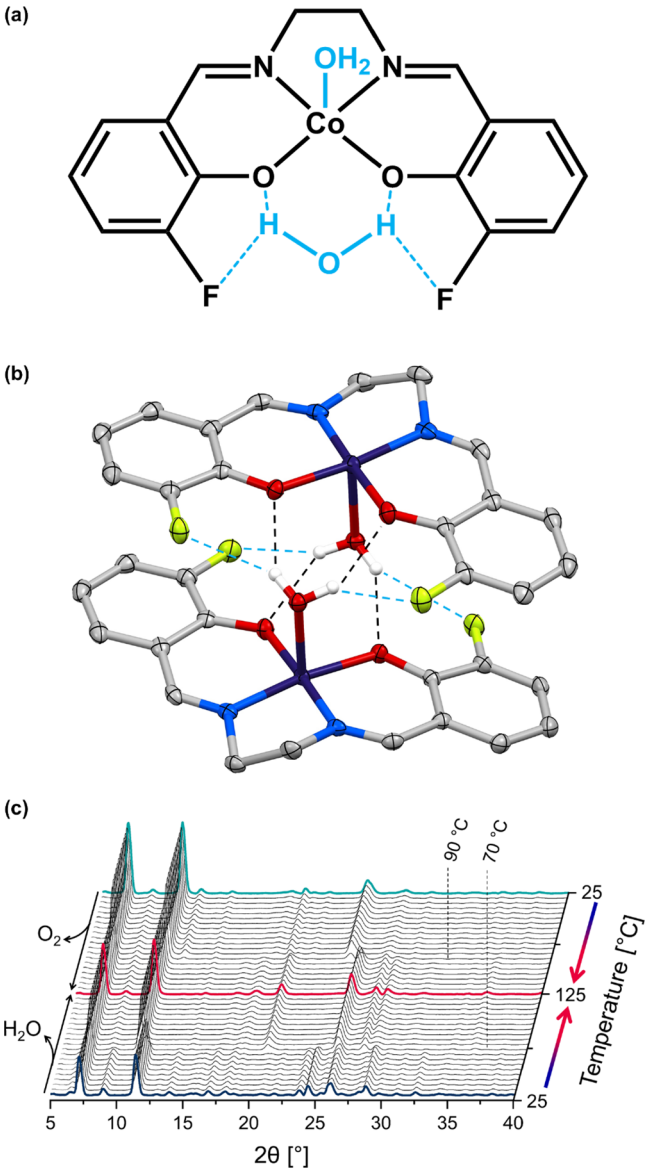

Figure 7. (a) Two ways in which water can associate with the Co(3F-salen) scaffold. (b) Crystal structure of Co(3F-salen)(H_2O) (**13**). Thermal ellipsoids drawn at 50% probability and H atoms bound to C are removed for clarity. Gray = carbon, red = oxygen, blue = nitrogen, white = hydrogen, yellow = fluorine, and indigo = cobalt. (c) VT-PXRD patterns recorded during stepwise heating of Co(3F-salen)-(H_2O) (**13**, blue) and α-Co(3F-salen)$(O_2)_{1/2}$ (**15**, teal). Both processes form α-Co(3F-salen) (**14**, red).

mechanisms behind the original observations made by Calvin and co-workers. Although the O_2 active solids obtained by thermal desorption of the pyridine and piperidine are ostensibly both "Co(3F-salen)", *i.e.*, the same formulation as produced through dehydration of the hydrates, inexplicably, the kinetics of the O_2 sorption depended on the formulation of the original starting material. The phase that was derived from the "piperidinate" sorbed O_2 faster than all of the other deoxygenated phases. Our structural analyses of these materials, which we believe to be identical based on observation of identical sorption/desorption properties, show that pyridine and piperidine are apical ligands in Co(3F-salen)py (**16**) and Co(3F-salen)pip·(H_2O) (**19**) (Figure 8 and Table S2). The geometries around the cobalt atoms of **16** and

https://doi.org/10.1021/jacsau.3c00134
JACS Au 2023, 3, 1484−1495

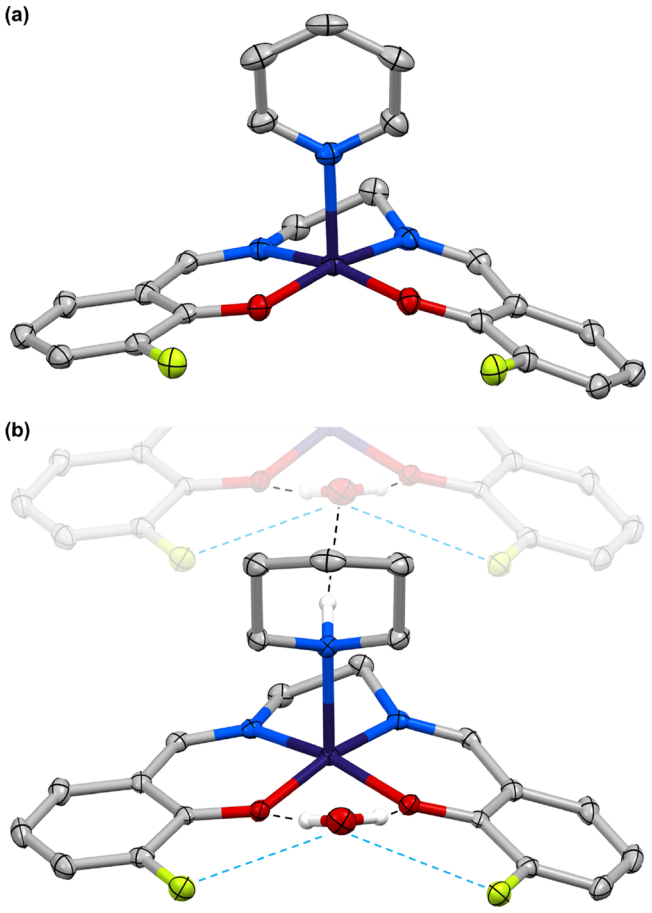

Figure 8. Crystal structures of (a) Co(3F-salen)py (**16**) and (b) Co(3F-salen)pip·(H_2O) (**19**). Thermal ellipsoids are drawn at 50% probability, and H atoms bound to C are omitted for clarity. Gray = carbon, red = oxygen, blue = nitrogen, white = hydrogen, yellow = fluorine, and indigo = cobalt.

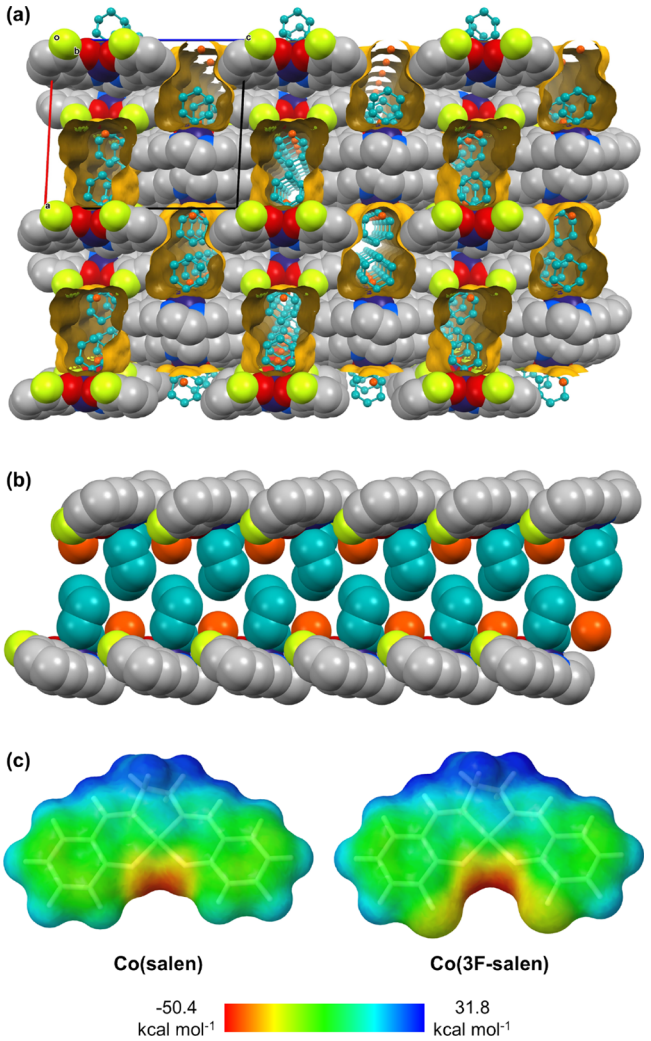

Figure 9. (a) Channels created by desorption of the coordinated piperidine from Co(3F-salen)pip·(H_2O) (**19**). The gold-colored surfaces represent the voids generated by in silico removal of the coordinated piperidines (teal) and the uncoordinated waters (orange). (b) Side view of the channels in **19** showing the packing of the piperidine (teal) and water (orange) molecules. (c) Electrostatic potential maps for Co(salen) (right) and Co(3F-salen) (left) mapped on the molecular solvent-accessible isosurface. The red and blue surfaces represent negative and positive regions of the potential, respectively.

19 are almost ideally square pyramidal as the angles deviate on average at 2.48 and 2.74° from 90°, while the cobalt atoms lie only 0.20 and 0.18 Å over the ONNO plane, respectively. There is, however, an interesting difference between **16** and **19** despite analogous preparation: A co-crystallized water in **19** is embraced by the two fluorine atoms and H-bonded to the phenoxy oxygen atoms of the same molecule (Figure 8b). A very weak interaction with the piperidine amine of an adjacent molecule is also present (O_{ph}···H−OH 2.15 Å, C−F···H−OH 2.50 Å, and N−H···OH_2 2.99 Å). The presence of a water molecule in the "piperidinate" (phase **19**) was not recognized in the original work.[13] Additionally, **19** undergoes a phase change upon cooling to 100 K (Supporting Information, page 5, Figure S13). The calculated powder pattern of the room temperature single-crystal structure fits nicely with the pattern of the powdered sample (Figure S11).

In silico removal of the pyridine or piperidine and water molecules from the crystal structures of **16** and **19**, respectively, results in the formation of channels through the structure parallel to the *b* axis like those proposed for the crystal structure of **11**. Accordingly, the Co(3F-salen) molecules interlock in a Flemish bond brick pattern (Figure 9a and Figure S10). While the intermolecular Co···Co distances in the structures of **10**, **16**, and **19** are practically identical, a significant contrast to the interior environment in ζ-Co(salen) (**11**) is the interior walls of the putative O_2 conduits in **17** and **20**, which are partially covered with organofluorine groups. In both structures, the major part of the electron density is localized in a cavity around the phenoxy oxygens due to the uncoordinated lone pairs. However, in Co(3F-salen), there is a lower electron density on the ethylene backbone due to the electron withdrawing fluorine atoms. A consequence will be that the imine groups in the 3F-salen scaffold will be less vulnerable toward oxidation. In addition, the substitution of hydrogen for fluorine atoms in the **3** position leads to a more evenly charged void surface and this is expected to facilitate movement of O_2 through the structure. A similar effect was described recently for the efficient transport of water molecules through supramolecularly polymerized nanorings within phospholipid bilayer membranes, which form fluorine-lined nanochannels.[64] Likewise, fluorination of a supramolecular transmembrane ion channel leads to increased selectivity for potassium over other alkali metal ions.[65] Using

https://doi.org/10.1021/jacsau.3c00134
JACS Au 2023, 3, 1484−1495

DFT at the M06L/def2-TZVP level of theory, electrostatic potential maps for Co(salen) and Co(3F-salen) were calculated (Figure 9c) and illustrate the effect.

The activation of **19** is best achieved by vacuum heating (140 °C and 0.05 mbar) to yield γ-Co(3F-salen) (**20**). The disappearance of prominent bands at 3436, 3227, and 3197 cm^{-1} assigned to water O−H and amine N−H vibrations in IR spectra suggests that both the water and the coordinated piperidine are desorbed during this process (Figure S14). TGA indicates that this occurs in a stepwise fashion with the water desorption occurring between 65 and 85 °C and the piperidine desorption between 105 and 165 °C (Figure S15). The powder pattern of **20** (Figure 10) fits with the powder X-ray

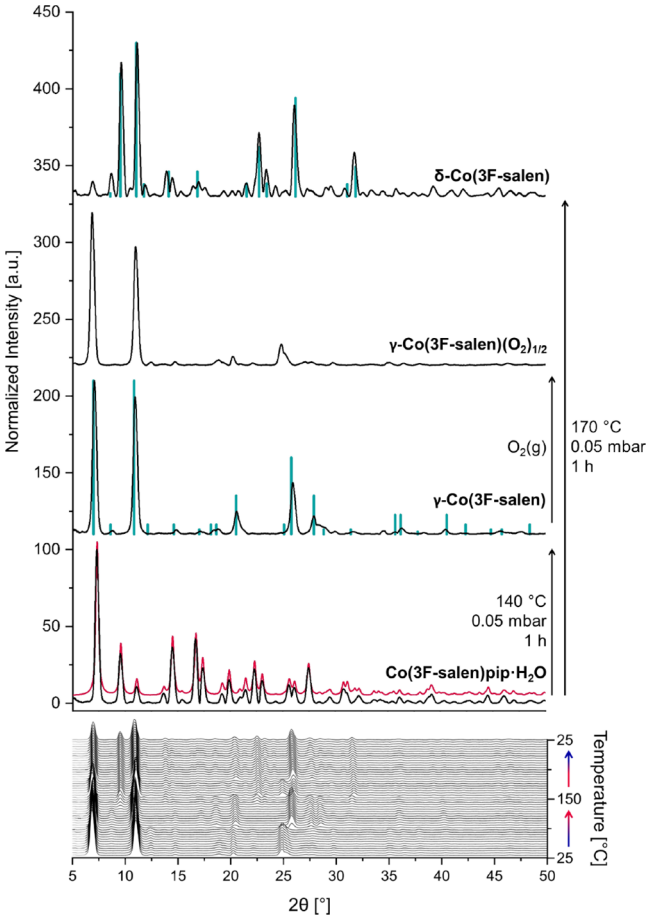

Figure 10. Powder patterns of the phases originating from activation of Co(3F-salen)pip·(H_2O) to form the O_2 active γ-Co(3F-salen), oxygenation to give γ-Co(3F-salen)$(O_2)_{1/2}$, or deactivation to δ-Co(3F-salen) (**19**), red line = calculated powder pattern and teal sticks = powder data reported by Calvin[4] (top). A description of how these data were translated into the teal sticks can be found in the Supporting Information (Tables S3 and S4). VT-PXRD patterns for heating to 150 °C and the subsequent cooling to 25 °C of γ-Co(3F-salen)$(O_2)_{1/2}$ (**21**) (bottom).

diffraction data of an oxygen active phase described in a patent from 1950[4] (Tables S3 and S4) for the material derived from thermal-vacuum activation of the "piperidinate" (*i.e.*, phase **19**).

This deoxygenated phase was shown to undergo 1500 sorption/desorption cycles during which time it lost 32% of its original activity.[9] When exposed to oxygen, **20** chemisorbs 1 mol of O_2 per 2 moles of cobalt very rapidly while changing color from red to jet black (Figure S16). Like **14**, the oxygen uptake by **20** is almost instantaneous; however, unlike **14**, the rate of oxygenation does not decrease over time and **20** is fully oxygenated to give γ-Co(3F-salen)$(O_2)_{1/2}$ (**21**) within minutes. In turn, **21** reverts to **20** when heated in a stream of nitrogen to 90 °C. It was originally noted that the O_2 active material (**20**) should not be heated to temperatures over 160 °C since this resulted in the loss of the O_2 sorptive property.[13] Consistent with these original observations, we found that further heating to 150 °C induces another phase change to a material, which is only partially active toward oxygen. Further heating to 170 °C under vacuum completely deactivates the materials and yields δ-Co(3F-salen) (**22**), which is completely inactive toward oxygenation. Again, the powder pattern of **22** matches nicely with the data for the inactive phase reported (Figure 10).[4]

In the solution state, deterioration of the reversible O_2 binding is mostly due to the irreversible oxidation of Co^{II} to Co^{III}. By contrast, Calvin *et al.* detected salicylic acid, hinting at oxidation of the imine bond[7,9,12] and suggesting that the solid-state deterioration is primarily due to the irreversible oxidation of the ligand. Co(3F-salen) was shown to have a higher cycling stability compared with Co(salen).[9] The fluorinated skeleton may be significant for making the imines in this structure less vulnerable toward oxidation since not only are the fluorine groups electron-withdrawing but they also physically shield the vulnerable imine bond (Figure 9b). This can explain why Co(3F-salen) has a higher cycling stability, compared to Co(salen).[9]

CONCLUSIONS

The discovery of an energy-efficient material for the swing absorption of O_2 remains highly sought for a wide range of applications from O_2 supplies to COPD patients, to aircraft and submarine emergency O_2 supplies, and for separation from H_2 in water electrolysis to name just a few. The typical energy consumption in units for the cryogenic separation of O_2 from air exceeds 200 kWh of electricity per ton of produced oxygen[66−69] and is thus associated with significant environmental impact.[70,71] Despite the eight intervening decades since Calvin and co-worker's impressive studies using 42 variations on the Co(salen) scaffold, and which were deemed highly important for the U.S. National Defense, no advance has been made. At that time, however, no SAR insight through crystallographic characterization was possible. Bulk homogeneity was also uncertain. Our reinvestigation of these materials has identified important SARs, and we describe how specific phase-pure materials can be prepared with bulk homogeneity. We have divided the O_2 binding phases of the Co(3R-salen) scaffold into two distinct classes, I and II:

Class I

These are phases that contain co-crystallized solvent molecules ($CHCl_3$, benzene, and CH_2Cl_2), which template hydrophobic O_2 transport conduits. Upon facile desolvation (under even ambient conditions), materials capable of selective O_2 absorption are generated. These phases do not achieve the theoretical maximum O_2 uptake.

Class II

These are storable air-stable phases that contain a coordinating solvent-derived axial ligand (pyridine, piperidine, and water), which can be chemi-desorbed using vacuum activation at temperatures around 140 °C. These form topologically

https://doi.org/10.1021/jacsau.3c00134
JACS Au 2023, 3, 1484−1495

different channels to those of Class I, and in the case of **10**, **16**, and **19**, these show an interlocked Flemish bond brick pattern. This class shows the highest O_2 capacity, chemisorbing 1 mol of O_2 per 2 moles of cobalt. Within this class, the fluorine-substituted systems offer a significant advantage. Fluorine-lined O_2 conduits will furnish a repulsive interaction with the guest O_2 molecules, thereby facilitating faster transport. In addition, the fluorine atoms form steric barriers as well as electronic protection of the ligand from destructive oxidation.

In addition, an irreproducible, but highly active, "monohydrate of Co(3F-salen)" was produced in the original work. We postulate that the superstructure of **19**, with its water binding pocket furnished by the juxtaposed phenol and organofluorine groups, might rationalize these original observations. Conceivably, this elusive highly active hydrate contains a water motif analogous to that in **19**, and a water molecule might be involved in a cooperative O_2 uptake mechanism.

We have reverse crystal-engineered the landmark Co(salen) scaffold to demonstrate principals for solid-state design of the materials that reach a maximum capacity of 1:2 O_2:[Co] stoichiometries. Although a considerable amount of research has involved the study of electronically tuned derivatives of Co(salen) in the solution state, it is solid-state materials that are sought for practical applications for use in filters and other applications. To this end, attempts have been made to immobilize the Co(salen) into porous copolymers[72,73] and onto nanoparticles.[74] Evidence for cyclability is also limited for these materials. Ultimately, however ,these conjugates will never achieve the O_2 densities possible to the crystalline solid state. The crystal phase presents a formidable tuning potential and one that can clearly override electronic tweaking. The long overdue results we describe here clearly show that molecules and phase design are synergic for enhanced O_2 storage and swing absorption in solid-state Co-based materials.

■ ASSOCIATED CONTENT

Supporting Information

The Supporting Information is available free of charge at https://pubs.acs.org/doi/10.1021/jacsau.3c00134.

Detailed experimental methods, materials synthesis and characterization, computational details, IR spectra, TGA, calculated PXRDs, details of SC X-ray structures, and additional crystal structures (PDF)

Accession Codes

CCDC 2241119 to 2241124 contain the supplementary crystallographic data for this paper. These data can be obtained free of charge via www.ccdc.cam.ac.uk/data_request/cif, by emailing data_request@ccdc.cam.ac.uk, or by contacting the Cambridge Crystallographic Data Centre, 12 Union Road, Cambridge CB2 1EZ, UK; fax: +441223 336033.

■ AUTHOR INFORMATION

Corresponding Author

Christine J. McKenzie − *Department of Physics, Chemistry and Pharmacy, University of Southern Denmark, 5230 Odense M, Denmark;* orcid.org/0000-0001-5587-0626; Email: mckenzie@sdu.dk

Author

Mads Sondrup Møller − *Department of Physics, Chemistry and Pharmacy, University of Southern Denmark, 5230 Odense M, Denmark;* orcid.org/0000-0003-1674-7742

Complete contact information is available at: https://pubs.acs.org/10.1021/jacsau.3c00134

Author Contributions

M.S.M. performed the practical work and wrote the first draft of the manuscript. C.J.M. procured funding for the work, provided guidance, and edited the manuscript.

Funding

This work was supported by the Danish Council for Independent Research | Technology and Production (grant 9041-00170B to C.J.M.).

Notes

The authors declare no competing financial interest.

■ ACKNOWLEDGMENTS

We thank Professor Vickie McKee for advice on the crystal structure determinations.

■ REFERENCES

(1) Pfeiffer, P.; Breith, E.; Lübbe, E.; Tsumaki, T. Tricyclische orthokondensierte Nebenvalenzringe. *Justus Liebigs Ann. Chem.* **1933**, *503*, 84−130.

(2) Tsumaki, T. N. IV. Über einige innerkomplexe Kobaltsalze der Oxyaldimine. *Bull. Chem. Soc. Jpn.* **1938**, *13*, 252−260.

(3) The National Defense Research Committee. *Science* **1940**, *92*, 599.

(4) Calvin, M. Cobalt bis-(3-fluorosalicylaldehyde)-ethylenediimine and method of making same. US 2, 493, 654 A, January 3, 1950.

(5) Calvin, M. Cobalt salicylaldehydeethylenediimine and method of production. US 2,508,490 A, May 23, 1950.

(6) Martell, A. E.; Calvin, M. *Chemistry of the Metal Chelate Compounds* ; Prentice-Hall, Inc., 1962.

(7) Calvin, M.; Bailes, R. H.; Wilmarth, W. K. The Oxygen-carrying Synthetic Chelate Compounds.[1a] I. *J. Am. Chem. Soc.* **1946**, *68*, 2254−2256.

(8) Barkelew, C. H.; Calvin, M. Oxygen-carrying Synthetic Chelate Compounds. II. The Rates of Oxygenation of the Solid Compounds[1]. *J. Am. Chem. Soc.* **1946**, *68*, 2257−2262.

(9) Wilmarth, W. K.; Aranoff, S.; Calvin, M. The Oxygen-carrying Synthetic Chelate Compounds. III. Cycling Properties and Oxygen Production[1]. *J. Am. Chem. Soc.* **1946**, *68*, 2263−2266.

(10) Calvin, M.; Barkelew, C. H. The Oxygen-carrying Synthetic Chelate Compounds. IV. Magnetic Properties[1]. *J. Am. Chem. Soc.* **1946**, *68*, 2267−2273.

(11) Hughes, E. W.; Wilmarth, W. K.; Calvin, M. The Oxygen-carrying Synthetic Chelate Compounds. V. Equilibrium with the Solid Compounds[1a]. *J. Am. Chem. Soc.* **1946**, *68*, 2273−2278.

(12) Harle, O. L.; Calvin, M. The Oxygen-Carrying Synthetic Chelate Compounds. VI. Equilibrium in Solution. *J. Am. Chem. Soc.* **1946**, *68*, 2612−2618.

(13) Bailes, R. H.; Calvin, M. The Oxygen-carrying Synthetic Chelate Compounds. VII. Preparation[1]. *J. Am. Chem. Soc.* **1947**, *69*, 1886−1893.

(14) Vogt, L. H.; Faigenbaum, H. M.; Wiberly, S. E. For several months during WWII the U. S. Navy produced oxygen aboard a destroyer depot ship for welding and cutting using a Co(salen)-based oxygen carrier complexes. The cost did not exceed that of cylinder oxygen, but the process had to be discontinued due to a shortage of cobalt. *Chem. Rev.* **1963**, *63*, 269−277.

(15) Stewart, R. F.; Estep, P. A.; Sebastian, J. J. S. In 1959 a survey was carried out by the Bureau of Mines to determine the economics

of production of tonnage quantities of oxygen, for the gasification of coal, utilizing Co(salen)-based oxygen carrier complexes. They concluded that the process was not economical for such large quantities of oxygen. *U.S. Bur. Mines Inform. Circ.* **1959**, *7906*.
(16) In recent years methods for oxygen separation utilising Co(salen) and compounds derived from it have been patented. US 6,436,171 B1.
(17) Niswander, R. H.; Taylor, L. T. ESR studies of cobalt dioxygen complexes containing pentadentate schiff base ligands. *J. Magn. Reson.* **1977**, *26*, 491−503.
(18) Floriani, C.; Fachinetti, G. Sodium [NN′-ethylenebis-(salicylideneiminato)cobaltate(I)], a reversible carbon dioxide carrier. *J. Chem. Soc., Chem. Commun.* **1974**, 615−616.
(19) Fachinetti, G.; Floriani, C.; Zanazzi, P. F. Bifunctional activation of carbon dioxide. Synthesis and structure of a reversible carbon dioxide carrier. *J. Am. Chem. Soc.* **1978**, *100*, 7405−7407.
(20) Floriani, C.; Calderazzo, F. Oxygen adducts of Schiff's base complexes of cobalt prepared in solution. *J. Chem. Soc., A* **1969**, 946.
(21) Nishinaga, A.; Tomita, H.; Nishizawa, K.; Matsuura, T.; Ooi, S.; Hirotsu, K. Regioselective formation of peroxyquinolatocobalt(III) complexes in the oxygenation of 2,6-di-t-butylphenols with cobalt(II) Schiff-base complexes. *J. Chem. Soc., Dalton Trans.* **1981**, 1504.
(22) Peretti, K. L.; Ajiro, H.; Cohen, C. T.; Lobkovsky, E. B.; Coates, G. W. A highly active, isospecific cobalt catalyst for propylene oxide polymerization. *J. Am. Chem. Soc.* **2005**, *127*, 11566−11567.
(23) Møller, M. S.; Kongsted, J.; McKenzie, C. J. Preparation of organocobalt(iii) complexes via O2 activation. *Dalton Trans.* **2021**, *50*, 4819−4829.
(24) Møller, M. S.; Liljedahl, M. C.; McKee, V.; McKenzie, C. J. Solid phase nitrosylation of enantiomeric cobalt(ii) complexes. *Chemistry* **2021**, *3*, 585−597.
(25) Jeon, J. Y.; Lee, J. J.; Varghese, J. K.; Na, S. J.; Sujith, S.; Go, M. J.; Lee, J.; Ok, M.-A.; Lee, B. Y. CO2/ethylene oxide copolymerization and ligand variation for a highly active salen-cobalt(III) complex tethering 4 quaternary ammonium salts. *Dalton Trans.* **2013**, *42*, 9245−9254.
(26) Hewlett, P. C.; Larkworthy, L. F. 161. Bridging water in the oxygen-carrying NN′-ethylenebis-(salicylideneiminato)cobalt(II) complex. *J. Chem. Soc.* **1965**, *0*, 882−885.
(27) Ochiai, E. The electronic configuration and oxygenation of NN′-ethylenebis(salicylaldehydeiminato)cobalt(II) studied by electron spin resonance spectroscopy. *J. Chem. Soc., Chem. Commun.* **1972**, 489−490.
(28) Chen, D.; Martell, A. E. Dioxygen affinities of synthetic cobalt Schiff base complexes. *Inorg. Chem.* **1987**, *26*, 1026−1030.
(29) Appleton, T. G. Oxygen uptake by a cobalt(II) complex. An undergraduate experiment. *J. Chem. Educ.* **1977**, *54*, 443.
(30) Calligaris, M.; Nardin, G.; Randaccio, L. The structure of the 1:2 adduct of oxygen with NN′-ethylene-bis(salicylaldehydeiminato)-cobalt(II) containing dimethylformamide. *J. Chem. Soc. D* **1969**, *0*, 763−764.
(31) Wang, B. C.; Schaefer, W. P. Structure of an oxygen-carrying cobalt complex. *Science* **1969**, *166*, 1404−1406.
(32) Lindblom, L. A.; Schaefer, W. P.; Marsh, R. E. The crystal and molecular structure of *μ*-peroxo-bis-[3,3′-diimino-di-*n*-propylamine-bis(salicylaldehyde)cobalt(III)].$C_6H_5CH_3$. *Acta Crystallogr., B Struct. Sci.* **1971**, *27*, 1461−1467.
(33) Schaefer, W. P.; Huie, B. T.; Kurilla, M. G.; Ealick, S. E. Oxygen-carrying cobalt complexes. 10. Structures of N,N'-ethylenebis(3-tert-butylsalicylideniminato)cobalt (II) and its monomeric dioxygen adduct. *Inorg. Chem.* **1980**, *19*, 340−344.
(34) Gall, R. S.; Rogers, J. F.; Schaefer, W. P.; Christoph, G. G. The structure of a monomeric oxygen carrying cobalt complex: dioxygen-N,N'-(1,1,2,2-tetramethyl)ethylenebis(3-tert-butylsalicylideniminato)-(1-benzylimidazole)cobalt(II). *J. Am. Chem. Soc.* **1976**, *98*, 5135−5144.
(35) Avdeef, A.; Schaefer, W. P. Reversible oxygen carriers. The synthesis and low temperature (−171.degree.) structure of an unstable monomeric dioxygen adduct of N,N'-(1,1,2,2-tetramethyl)-ethylenebis(3-fluorosalicylideniminato)(1-methylimidazole)cobalt-(II), Co(3-F-Saltmen)(1-Me-Imid)(O2).2Me2CO. *J. Am. Chem. Soc.* **1976**, *98*, 5153−5159.
(36) Carré, F.; Corriu, R. J. P.; Lancelle-Beltran, E.; Mehdi, A.; Reyé, C.; Guilard, R.; Sýkora, J.; van der Lee, A. X-Ray crystal structures of copper(ii) and cobalt(ii) complexes with Schiff base ligands. Reactivity towards dioxygen. *Dalton Trans.* **2003**, 3211−3215.
(37) Gall, R. S.; Schaefer, W. P. Preparation and structural characterization of a monomeric dioxygen adduct of (N,N'-(1,1,2,2-tetramethylethylene)bis(salicylideneiminato))-(1-benzylimidazole)-cobalt(II). *Inorg. Chem.* **1976**, *15*, 2758−2763.
(38) Huie, B. T.; Leyden, R. M.; Schaefer, W. P. Oxygen-carrying cobalt complexes. 9. Preparation and crystal structure of the dioxygen adduct of aquo[N,N'-(1,1,2,2-tetramethylethylene)bis(3-methoxysalicylideneiminato)]cobalt(II). *Inorg. Chem.* **1979**, *18*, 125−129.
(39) Cini, R.; Orioli, P. Crystal and molecular structure of the reversible dioxygen adduct of [NN′-4-methyl-4-azaheptane-1,7-diylbis(salicylideneiminato)]cobalt(II). *J. Chem. Soc., Dalton Trans.* **1983**, 2563−2568.
(40) Collman, J. P.; Takaya, H.; Winkler, B.; Libit, L.; Koon, S. S.; Rodley, G. A.; Robinson, W. T. General syntheses for new pentadentate ligands. Crystal structure of *α*,*α*'-{2-(2′-pyridyl)ethyl}-ethylenebis(salicylideniminato)cobalt(II)-ethanol. *J. Am. Chem. Soc.* **1973**, *95*, 1656−1657.
(41) Jameson, G. B.; Robinson, W. T.; Rodley, G. A. Crystal and molecular structure of (dioxygen){NN′-[2-(2′-pyridyl)ethyl]-ethylenebis(salicylideneiminato)}cobalt−acetonitrile (1/1). *J. Chem. Soc., Dalton Trans.* **1978**, 191−196.
(42) Cini, R.; Orioli, P. X-Ray structure of the reversible dioxygen adduct of [N,N′-(3,3′-dipropylmethylamine)bis-(salicylideneaminato)cobalt(II)]: unusual presence of both dioxygenated and non-dioxygenated complex molecules in the crystal. *J. Chem. Soc., Chem. Commun.* **1981**, 196−198.
(43) Chai, S. W.; Kothare, M. V.; Sircar, S. Rapid pressure swing adsorption for reduction of bed size factor of a medical oxygen concentrator. *Ind. Eng. Chem. Res.* **2011**, *50*, 8703−8710.
(44) Southon, P. D.; Price, D. J.; Nielsen, P. K.; McKenzie, C. J.; Kepert, C. J. Reversible and selective O2 chemisorption in a porous metal-organic host material. *J. Am. Chem. Soc.* **2011**, *133*, 10885−10891.
(45) Sundberg, J.; Cameron, L. J.; Southon, P. D.; Kepert, C. J.; McKenzie, C. J. Oxygen chemisorption/desorption in a reversible single-crystal-to-single-crystal transformation. *Chem. Sci.* **2014**, *5*, 4017−4025.
(46) Brückner, S.; Calligaris, M.; Nardin, G.; Randaccio, L. The crystal structure of the form of N,N'-ethylenebis-(salicylaldehydeiminato)cobalt(II) inactive towards oxygenation. *Acta Crystallogr. B Struct. Crystallogr. Cryst. Chem.* **1969**, *25*, 1671−1674.
(47) Yuan, W.-B.; Wang, H.-Y.; Du, J.-F.; Chen, S.-W.; Zhang, Q. 2,2′-Ethane-1,2-diylbisnitrilomethylidenediphenolatocobalt(II). *Acta Crystallogr. E, Struct. Rep. Online* **2006**, *62*, m3504−m3505.
(48) Schaefer, W. P.; Marsh, R. E. Oxygen-carrying cobalt compounds. I. Bis(salicylaldehyde)ethylenediiminecobalt(II) monochloroformate. *Acta Crystallogr. B Struct. Sci.* **1969**, *25*, 1675−1682.
(49) Holt, S. L.; DeIasi, R.; Post, B. Crystal structure of the oxygen-inactive form of bis(salicylaldehyde)ethylenediiminecobalt(II). *Inorg. Chem.* **1971**, *10*, 1498−1500.
(50) Calligaris, M.; Minichelli, D.; Nardin, G.; Randaccio, L. Structural aspects of the synthetic oxygen-carrier NN′-ethylenebis-(salicylideneiminato)cobalt(II). Part II. Crystal and molecular structure of the monopyridine complex. *J. Chem. Soc. A* **1970**, *0*, 2411−2415.
(51) Macrae, C. F.; Sovago, I.; Cottrell, S. J.; Galek, P. T. A.; McCabe, P.; Pidcock, E.; Platings, M.; Shields, G. P.; Stevens, J. S.; Towler, M.; Wood, P. A. Mercury 4.0: from visualization to analysis, design and prediction. *J. Appl. Crystallogr.* **2020**, *53*, 226−235.

https://doi.org/10.1021/jacsau.3c00134
JACS Au 2023, 3, 1484−1495

(52) Schlesinger, C.; Fitterer, A.; Buchsbaum, C.; Habermehl, S.; Chierotti, M. R.; Nervi, C.; Schmidt, M. U. Ambiguous structure determination from powder data: four different structural models of 4,11-di-fluoro-quinacridone with similar X-ray powder patterns, fit to the PDF, SSNMR and DFT-D. *IUCrJ* **2022**, *9*, 406−424.
(53) Kumar, S.; Gupta, R. Endogenous and Exogenous Ligand-Dependent Formation of a Superoxide-Bridged Dicobalt(III) Complex and Mononuclear Co^{III} Complexes with Amide-Based Macrocyclic Ligands. *Eur. J. Inorg. Chem.* **2014**, *2014*, 5567−5576.
(54) Timmons, J. H.; Niswander, R. H.; Clearfield, A.; Martell, A. E. Crystal and molecular structure of μ-peroxo-bis[(1,9-bis(2-pyridyl)-2,5,8-triazanonane)cobalt(III)] tetraiodide. Effect of chelate ring size on the structures and stabilities of dioxygen complexes. *Inorg. Chem.* **1979**, *18*, 2977−2982.
(55) Lewis, G. R.; Wilson, C. μ-Peroxo-bis[*trans* -chloro(1,4,8,11-tetraazacyclotetradecane)cobalt(III)] bis(tetraphenylborate) diacetone solvate. *Acta Crystallogr., C Cryst. Struct. Commun.* **2001**, *57*, 1159−1161.
(56) Timmons, J. H.; Clearfield, A.; Martell, A. E.; Niswander, R. H. Crystal and molecular structure of μ-peroxo-bis{[1,11-bis(2-pyridyl)-2,6,10-triazaundecane]cobalt(III)} tetraiodide trihydrate. A cobalt dioxygen complex of a pentadentate ligand. *Inorg. Chem.* **1979**, *18*, 1042−1047.
(57) Calligaris, M.; Nardin, G.; Randaccio, L.; Ripamonti, A. Structural aspects of the synthetic oxygen-carrier NN′-ethylenebis(salicylideneiminato)cobalt(II): structure of the addition compound with oxygen containing dimethylformamide. *J. Chem. Soc. A* **1970**, *0*, 1069−1074.
(58) Suzuki, M.; Ishiguro, T.; Kozuka, M.; Nakamoto, K. Resonance Raman spectra, excitation profiles, and infrared spectra of [N,N'-ethylenebis(salicylideniminato)]cobalt(II) in the solid state. *Inorg. Chem.* **1981**, *20*, 1993−1996.
(59) Freedman, T. B.; Yoshida, C. M.; Loehr, T. M. Resonance Raman spectra of μ-peroxo binuclear cobalt(III) complexes. *J. Chem. Soc., Chem. Commun.* **1974**, 1016−1017.
(60) Nakamoto, K.; Suzuki, M.; Ishiguro, T.; Kozuka, M.; Nishida, Y.; Kida, S. Resonance Raman spectra of molecular oxygen adducts of N,N'-ethylenebis(salicylideniminato)cobalt(II), [BCo(salen)]2O2 (B = pyridine, pyridine N-oxide, and dimethylformamide). *Inorg. Chem.* **1980**, *19*, 2822−2824.
(61) Maxwell, J. C.; Volpe, J. A.; Barlow, C. H.; Caughey, W. S. Infrared evidence for the mode of binding of oxygen to iron of myoglobin from heart muscle. *Biochem. Biophys. Res. Commun.* **1974**, *58*, 166−171.
(62) Kozuka, M.; Nakamoto, K. Vibrational studies of (tetraphenylporphyrinato)cobalt(II) and its adducts with carbon monoxide, nitric oxide, and oxygen in gas matrixes. *J. Am. Chem. Soc.* **1981**, *103*, 2162−2168.
(63) Matthews, R. A. J. The Science of Murphy's Law. *Sci. Am.* **1997**, *276*, 88.
(64) Itoh, Y.; Chen, S.; Hirahara, R.; Konda, T.; Aoki, T.; Ueda, T.; Shimada, I.; Cannon, J. J.; Shao, C.; Shiomi, J.; Tabata, K. V.; Nijo, H.; Sato, K.; Aida, T. Ultrafast water permeation through nanochannels with a densely fluorous interior surface. *Science* **2022**, *376*, 738−743.
(65) Sato, K.; Sasaki, R.; Matsuda, R.; Nakagawa, M.; Ekimoto, T.; Yamane, T.; Ikeguchi, M.; Tabata, K. V.; Noji, H.; Kinbara, K. Supramolecular mechanosensitive potassium channel formed by fluorinated amphiphilic cyclophane. *J. Am. Chem. Soc.* **2022**, *144*, 11802−11809.
(66) Variny, M.; Jediná, D.; Rimár, M.; Kizek, J.; Kšiňanová, M. Cutting Oxygen Production-Related Greenhouse Gas Emissions by Improved Compression Heat Management in a Cryogenic Air Separation Unit. *Int. J. Environ. Res. Public Health* **2021**, *18*, 10370.
(67) Singla, R.; Chowdhury, K. Enhanced oxygen recovery and energy efficiency in a reconfigured single column air separation unit producing pure and impure oxygen simultaneously. *Chem. Eng. Process.* **2021**, *162*, No. 108354.
(68) Ghoniem, A. F.; Zhao, Z.; Dimitrakopoulos, G. Gas oxy combustion and conversion technologies for low carbon energy: Fundamentals, modeling and reactors. *Proc.Combust Inst.* **2019**, *37*, 33.
(69) Patzek, T. W.; Croft, G. D. Potential for Coal-to-Liquids Conversion in the United States—Fischer−Tropsch Synthesis. *Nat. Resour. Res.* **2009**, *18*, 181−191.
(70) Wang, Z.; Wang, W.; Qin, W.; Gui, W.; Xu, S.; Yang, C.; Zhang, Z.; Wang, Y.; Zheng, J.; Liu, X. Analysis of carbon footprint reduction for three novel air separation columns. *Sep. Purif. Technol.* **2021**, *262*, No. 118318.
(71) Cormos, C.-C. Techno-Economic Evaluations of Copper-Based Chemical Looping Air Separation System for Oxy-Combustion and Gasification Power Plants with Carbon Capture. *Energies* **2018**, *11*, 3095.
(72) Sharma, A. C.; Borovik, A. S. Design, synthesis, and characterization of templated metal sites in porous organic hosts: application to reversible dioxygen binding. *J. Am. Chem. Soc.* **2000**, *122*, 8946−8955.
(73) Welbes, L. L.; Borovik, A. S. Confinement of metal complexes within porous hosts: development of functional materials for gas binding and catalysis. *Acc. Chem. Res.* **2005**, *38*, 765−774.
(74) Johnson, C.; Ottiger, S.; Pini, R.; Gorman, E. M.; Nguyen, J. G.; Munson, E. J.; Mazzotti, M.; Borovik, A. S.; Subramaniam, B. Near-stoichiometric O_2 binding on metal centers in Co(salen) nanoparticles. *AIChE J.* **2009**, *55*, 1040−1045.

https://doi.org/10.1021/jacsau.3c00134
JACS Au 2023, 3, 1484−1495